Semnan University

Journal of Heat and Mass Transfer Research

Journal homepage: http://jhmtr.journals.semnan.ac.ir

Numerical modelling of double-diffusive natural convection within an arc-shaped enclosure filled with a porous medium

Ariyan Zare Ghadi*[1], Ali Haghighi Asl[2], Mohammad Sadegh Valipour[1]

[1]*School of Mechanical Engineering, Semnan University, Semnan, Iran*
[2]*School of Chemical Engineering, Semnan University, Semnan, Iran*

PAPER INFO

History:
Received 14 December 2013
Accepted 16 February 2014

Keywords:
FVM method
Double-diffusive convection
Arc-shaped cavity
Porous media

A B S T R A C T

Numerical study of double-diffusive natural convective heat transfer in a curved cavity filled with a porous medium has been carried out in the current study. Polar system has been selected as coordinate system. As a result, all equations have been discredited in r and θ directions. Brinkmann extended Darcy model has been utilized to express fluid flow in porous matrix in the enclosure. Smaller and larger curved walls are supposed to be hot and cold sources, respectively. Other two walls are insulated. The numerical solution has been obtained based on the finite volume methodology via staggered grid system, which will be explained in detail in its respective section. Finally, at the result section the effects of all pertinent parameters i.e. Grashof number, Lewis number, Darcy number, and Buoyancy ratio on the fluid motion and medium thermal behavior have been illustratively discussed. Results reveal that an increasing in Lewis number has a negative effect on heat transfer, while it has a positive impact on mass transfer. It is also seen that the flow intensity is increased by decreasing Lewis number. In addition, it is observed that for the aiding flow case, average Nu and Sh numbers decrease with increasing buoyancy ratio, while for opposing flow cases Nu and Sh augment with decreasing buoyancy ratio.

© 2014 Published by Semnan University Press. All rights reserved.

1. Introduction

Such condition in which the flow is driven by buoyancy force produced by combined act of thermal and concentration gradients is known as a double-diffusive convection. This phenomenon occurs in many industrial engineering and environmental applications such as drying processes, heat exchangers, chemical processes, energy storages, etc. There are noticeable studies reporting double-diffusive convection in non-porous enclosures, while only a few studies have investigated this phenomenon in a porous enclosure in the literature. Authors draw readers' attention to some more pertinent researches published in this field in the following paragraph.

Researches carried out by Hu and EL-Wakil [1], Ostrach [2- 4], and Lee et al. [5] are primary works related to blend of heat and mass transfer in enclosures. Nithiarasu et al. [6] studied double-diffusive natural convection in a porous enclosure with a freely convecting wall. Their effort exhibited a direct bearing of the buoyancy ratio on flow pattern and thermosolutal behavior. Double-diffusive natural convection in parallelogrammic enclosures filled with fluid-saturated porous media using the Darcy model has been investigated by Costa [7]. He has found that strong changes occur in the parallelogrammic enclosure when the Rayleigh number, the inclination angle, and the aspect ratio of the enclosure change. Goyeau et al. [8] reported a work on double-diffusive natural convection in a porous cavity using the Darcy-Brinkmann formulation. They indicate that the impact of the Darcy number on double-diffusion process is more complex than in thermal convection, and also the behavior has been already examined for fluids. Chamkha and Al-Mudhaf [9] carried out a work about the double-diffusive natural convection in a tilted porous cavity considering

Corresponding author: Ariyan Zare Ghadi, School of Mechanical Engineering, Semnan University, P.O.Box:35196-45399, Semnan, Iran. *Email: azghadi@semnan.ac.ir*

heat source or sink. They conclude that as the cavity angle increases the average Nusselt and Sherwood numbers decreases. They also find a critical angle for which the Sh and Nu numbers attain their maximum values. Eyden et al. [10] explored turbulent double-diffusive natural convection in trapezoidal enclosures. They had two main sections; temperature driven natural convection and combined temperature and mass driven natural convection. For the second case, they injected Argon and Nitrogen in the enclosure and studied the effects of injected rates on flow pattern and thermo-solutal behaviors. Bourich et al. [11] conducted a work on double-diffusive natural convection within a porous cavity partially heated from below and differentially salted. They find that the effect of buoyancy ratio on the heat, mass, and flow pattern depends on the kind of solution, the Lewis and Rayleigh numbers, and the location of the heat source. The range of buoyancy ratio for which a certain solution is maintained, depends on both Lewis number and Rayleigh number. Double-diffusive natural convection in a square enclosure with discrete heat sources has been reported by Teamah et al [12]. The results reveal that the average Nusselt number and average Sherwood number are amplified with an increment in the Rayleigh number, the dimensionless heater length, and Prandtl number. El Ayachi et al. [13], Bourich et al. [14], Teamah [15], Belazizia et al. [16] and Nikbakhti et al. [17] also reported related studies in this manner.

To the best knowledge of the authors, there is no study to examine double-diffusive natural convection in an arced cavity. This type of geometry is widely employed in the industrial and engineering applications such as underground electric transmission cables, thermal insulation, cryogenics, thermal energy storages, porous heat exchangers, and nuclear waste repositories. This gap in the literature motivates the authors to scrutinize the double-diffusive free convection in a fluid saturated arc-shaped porous enclosure.

2. Mathematical Modeling

2.1 Conceptual model

Figure 1 indicates the geometry used in this study. The enclosure has been filled with porous matrix. The fluid

flow is considered to be incompressible, steady, laminar, and two-dimensional with constant properties. The density varies in accordance with the Boussinesq model. The outer semi-circular wall acts as a cold source and the inner wall acts as a hot source. Two horizontal walls are insulated.

2.2 Governing equations

The two dimensional continuity, momentum, energy, and mass equations for laminar natural convection in polar coordinate system are as following [18]:

- Mass Continuity

$$\frac{1}{r}\frac{\partial(ru_r)}{\partial r}+\frac{1}{r}\frac{\partial u_\theta}{\partial \theta}=0 \tag{1}$$

- $\theta-$ Momentum Equation

$$\begin{aligned}&\frac{1}{\varepsilon}\left(\frac{u_\theta}{r}\frac{\partial u_\theta}{\partial \theta}+u_r\frac{\partial u_\theta}{\partial r}+\frac{u_\theta u_r}{r}\right)=-\varepsilon\frac{1}{r}\frac{\partial p}{\partial \theta}+\\&\Pr\left(\frac{1}{r}\frac{\partial}{\partial r}\left(r\frac{\partial u_\theta}{\partial r}\right)+\frac{1}{r^2}\frac{\partial^2 u_\theta}{\partial \theta^2}+\frac{2}{r^2}\frac{\partial u_r}{\partial \theta}-\frac{u_\theta}{r^2}\right)\\&-\varepsilon\frac{\Pr}{Da}u_\theta+Ra.\Pr.T.\sin\theta-N.Ra.\Pr.C.\sin\theta\end{aligned} \tag{2}$$

- $r-$ Momentum Equation

$$\begin{aligned}&\frac{1}{\varepsilon}\left(\frac{u_\theta}{r}\frac{\partial u_r}{\partial \theta}+u_r\frac{\partial u_r}{\partial r}-\frac{{u_\theta}^2}{r}\right)=-\varepsilon\frac{\partial p}{\partial r}+\\&\Pr\left(\frac{1}{r}\frac{\partial}{\partial r}\left(r\frac{\partial u_r}{\partial r}\right)+\frac{1}{r^2}\frac{\partial^2 u_r}{\partial \theta^2}-\frac{2}{r^2}\frac{\partial u_\theta}{\partial \theta}-\frac{u_r}{r^2}\right)\\&-\varepsilon\frac{\Pr}{Da}u_r+Ra.\Pr.T.\cos\theta-N.Ra.\Pr.C.\cos\theta\end{aligned} \tag{3}$$

- Energy Equation

$$\left(\frac{u_\theta}{r}\frac{\partial T}{\partial \theta}+u_r\frac{\partial T}{\partial r}\right)=\left(\frac{1}{r}\frac{\partial}{\partial r}\left(\frac{\partial T}{\partial r}\right)+\frac{1}{r^2}\frac{\partial^2 T}{\partial \theta^2}\right) \tag{4}$$

- Mass Equation

$$\left(\frac{u_\theta}{r}\frac{\partial C}{\partial \theta}+u_r\frac{\partial C}{\partial r}\right)=\frac{1}{Le}\left(\frac{1}{r}\frac{\partial}{\partial r}\left(\frac{\partial C}{\partial r}\right)+\frac{1}{r^2}\frac{\partial^2 C}{\partial \theta^2}\right) \tag{5}$$

- Auxiliary Equations

Some equations should be defined as following to evaluate the heat transfer rate, local and average Nusselt number, and Sherwood number:

$$Nu=\left(\frac{\partial T}{\partial r}\right)_{r=1}\quad\&\quad Sh=\left(\frac{\partial C}{\partial r}\right)_{r=1} \tag{6}$$

$$Nu_{ave}=\frac{1}{\pi}\int_0^\pi Nud\theta\quad\&\quad Sh_{ave}=\frac{1}{\pi}\int_0^\pi Shd\theta \tag{7}$$

Esq. 1-6 are in dimensionless form. The dimensionless variables may be defined as following:

$$r=\frac{r^*}{R},\quad \theta=\theta^*,\quad u_\theta=\frac{u_\theta^* R}{\alpha},\quad u_r=\frac{u_r^* R}{\alpha},$$
$$p=\frac{p^*}{\rho U_\infty{}^2},\quad T=\frac{T^*-T_\infty}{T_s-T_\infty},\quad Le=\frac{\nu}{D}$$
$$C=\frac{C^*-C_\infty}{C_s-C_\infty},\quad Da=\frac{K}{R^2},\quad N=\frac{\beta_C(C_s-C_\infty)}{\beta_T(T_s-T_\infty)},\qquad (8)$$
$$Ra=\frac{g\beta(T_s-T_\infty)R^3}{\nu\alpha},\quad \Pr=\frac{\nu}{\alpha}$$

The variable with superscript "*" denotes dimensional variables.

2.3 Boundary conditions

According to Fig. 1 the governing equations (1-4) are subjected to the following conditions:

$$r=R\ \ \&\ \ 0\le\theta\le\pi\Rightarrow\ u_\theta=0,\ u_r=0,\ T=0,\ C=0 \qquad (9)$$

$$r=2R\ \ \&\ \ 0\le\theta\le\pi\Rightarrow\ u_\theta=0,\ u_r=0,\ T=0,\ C=0 \qquad (10)$$

$$\theta=0,\pi\ \ \&\ \ R\le r\le 2R\Rightarrow\ u_\theta=0,\ u_r=0,\ \frac{\partial T}{\partial r}=0,\ \frac{\partial C}{\partial r}=0 \qquad (11)$$

3. Numerical Technique

The coupled governing continuity, momentum, energy, and concentration equations are discretized using the finite volume method (FVM). The coupling between velocity and pressure in momentum equation is accomplished by using the SIMPLE technique [19]. To discretize the equations, a combination of central difference and upwind methods is employed [20]. To make sure that the convergence occurs in the sequential iterative solution, the relative variations of definite variables between two successive iterations have been required to be less than the specified accuracy level of 10^{-6}.

A grid independence study has been examined for $\Pr=1$, $Da=10^{-4}$, $Ra=10^5$, $Le=0.1$, and $N=1$ to obtain average Sherwood number. Table 1 shows the effect of the number of grids on the average Sherwood number. The results reveal that the homogeneous grid system of 101×71 is acceptable to achieve precise result in the present study.

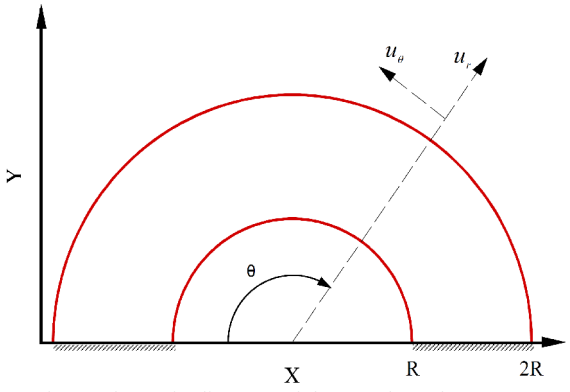

Fig.1 Schematic diagram of the arc-shaped porous enclosure

In order to validate our numerical solution, local results obtained by our code has been compared by the published results of Iwatsu et al. [21]. The engineering parameters for such validation are mimicked with the conditions as invoked by Iwatsu et al. [21]. They investigate heat and flow pattern in lid-driven square cavity with two insulated vertical walls while top wall is hot and bottom wall is cold. Comparison includes one graph and one table. In figure 2 Nusselt number at the top wall for Re=100 and Gr=10^6 has been compared between two works and a good agreement is seen. In table 2, the average Nusselt number at the top wall for Gr=100 at different Re has been compared and the errors has been calculated. These results also show good agreement between these two works.

4. Results and Discussion

In the present section, results are illustrated in the form of streamlines, isotherms, and iso-concentrations. Besides, graphs showing thermal and solutal behaviors of flow are exhibited in this section. All results have been obtained based on pertinent dimensionless parameters of Grashof number, Lewis number, Darcy number, and Buoyancy ratio. The ranges of varying parameters are $-10<N<10$, $10^3<Ra<10^5$, $0.1<Le<10$, whereas Darcy number and Prandtl number are fixed at 10^{-4} and 1, respectively. All findings are presented through the

Table 1: Effect of grid number on Sh_{ave} at $\Pr=1$, $Da=10^{-4}$, $Ra=10^5$, $Le=0.1$ and $N=1$

Number of Grids	Sh_{ave}	Error
41× 21	3.0108	
61× 41	2.9506	2%
91× 61	2.9329	0.6%
101× 71	2.9285	0.15%
151× 101	2.9259	0.09%

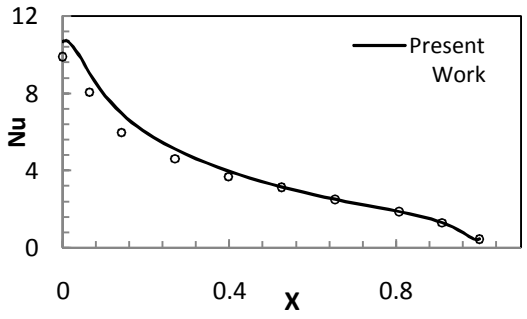

Fig.2 Comparison of the local Nusselt number between the present code and the results of Iwatsu et al. [21]

Table 2: Comparison of the Average Nu at the top wall between the present work and that of Iwatsu et al. [21] for Gr=100

Parameter	Present Work	Iwatsu et al. [21]	Error
Re=100	1.99	1.94	2.57 %
Re=400	3.90	3.84	1.56 %
Re=1000	6.42	6.33	1.42 %

following paragraphs.

Streamlines, temperature and concentration contours have been plotted in figure 3 for N=-5 and N=-10 at Le=10 and Ra=105. For these two buoyancy ratios, we meet aiding double-diffusive flow, because solutal buoyancy force amplifies thermal buoyancy force. Vortices are evidently strong as the maximum stream functions for N=-5 and -10 are 2.57 and 1.52, respectively. For aiding flow case, left hand vortices are clockwise and right hand vortices are counterclockwise. Temperature contours in the second line of the figure indicate that for N=-10 the thermal boundary layer on the two sides of hot curved wall are thinner than that for N=-5. As a result, the Nusselt number is higher in those areas for N=-10. On the contrary, the wall thermal boundary layer for N=-10 is thicker than that for N=-5 in the middle of hot curved. Concentration contours in the third line prove intense gradients of concentration near the corners of hot wall portraying narrow solutal boundary layer. In the middle of the wall, dense solutal boundary layers extending towards two sides are seen.

Figure 4 indicates pathlines, isotherms, and iso-concentrations for N=5 and N=10 at fixed Lewis number (Le=10) and fixed Rayleigh number (Ra=105). The figure shows opposing flow regime in which solutal buoyancy force opposes the thermal buoyancy force. In contrast to aiding flow, left hand vortices are counterclockwise and right hand vortices are clockwise in this case. As it is expected, the strength of the vortices is lower than that of aiding flow case, so that the maximum stream function for N=5 and 10 reaches 1.38 and 0.82, respectively. Temperature field exemplifies gradients more consistent than aiding flow. It is evident from the figure that the temperature field has been stratified in radial direction, especially for N=10. Concentration field can be seen in the tird line of the figure. Iso-concentration lines are more uniformed than those of aiding flow regime. Concentration gradients in the middle of the hot wall are much denser than the corners of it. This is because of the conflicting effect of solutal buoyancy force. It is worth to mention that N=0 ascribes to negligible species impacts expressing pure thermal convection and N=∞ refers to predominant solutal impacts.

Figure 5 represents the flow pattern, isotherms, and iso-concentrations for various Lewis numbers at fixed buoyancy ratio, Darcy number, and Rayleigh number. Flow intensity, which is characterized by the maximum stream function, is increased by decreasing the Lewis number. As shown in the figure $\psi_{max} = 1.85$ occurs in Le=10 and $\psi_{max} = 6.44$ occurs in Le=0.1. The figure also displays the vortices' core approaches horizontal walls by increasing Lewis number. Isotherms show uniform temperature distribution in the bulk of the cavity and increasing the Lewis numbers results in more uniform temperature distribution. The third line represents iso-concentrations which have an opposite behavior compared to the isotherms.

Figure 6 displays the contours for temperature and concentration for different values of Da, *Le*, and *Ra* numbers and for a fixed value of *N*. For $Da=10^{-4}$ (low Darcy number) the microscopic drag force is high and the fluid experiences a pronounced large resistance as it flows through the porous matrix, causing the flow to cease in the most of the cavity, which suppresses the buoyancy forces. In this case, an increase in Rayleigh number has an insignificant effect on heat and mass transfer because in higher *Ra* with natural convection dominated regime, porous matrix has a high resistance to the natural flow. Accordingly, the changes in isotherms and iso-concentrations are not remarkable in low Darcy number ($Da=10^{-4}$) as it can be seen in the figure. As the Darcy number increases ($Da=10^{-2}$), the resistance of porous medium decreases and the fluid easily flows in the cavity. In this case, by increasing the Rayleigh number the natural convection regime will be dominant and due to of low resistance of porous matrix, the alterations from conduction dominated regime to convection dominated one are totally noticeable in the figure.

Figure 6 also shows that at high Lewis number (Le=10) the Isotherms are almost parallel to the curved walls of cavity for nearly all values of Rayleigh numbers, indicating that most of the heat transfer is carried out by heat conduction. This is due to an increase in the thermal boundary-layer thickness. On the contrary, the iso-concentration contours are enhanced for higher Lewis number (Le=10). This happens because the solutal boundary-layer thickness decreases and consequently enhances thermo-solutal activities in the enclosure when the Lewis number increases.

Sherwood number and Nusselt number along the hot curved wall for various Lewis numbers and N=10 are depicted in figures 7 and 8. For both cases, the maximum value occurs in the middle of the cavity, whereas the minimum value occurs in angles 0 and 180 °. This happens because the denser gradients and accordingly thinner boundary layers take place in the middle of the cavity. The distinct difference between the two graphs is that the maximum value for *Sh* number increases with increasing *Le* number, whereas the maximum value for

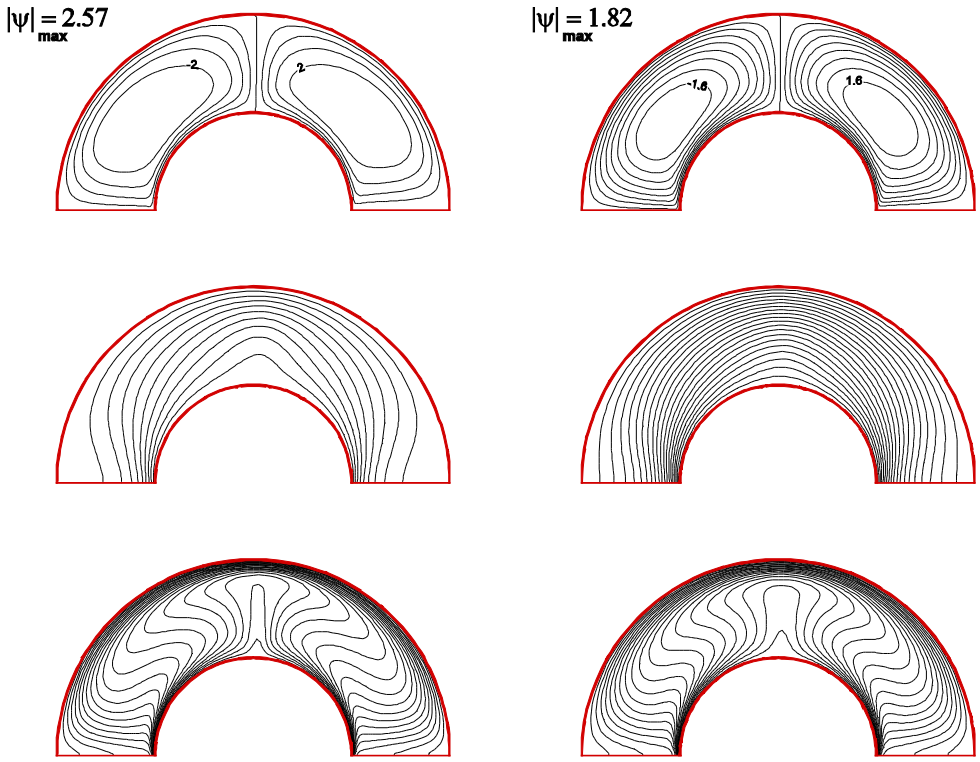

Fig.3 Streamlines (1st row), Isotherms (2nd row) and Iso-concentrations (3rd row) for *N*=-10 (left column) and *N*=-5 (right column) at *Le*=10, *Da*=1.e-4, and *Ra*=1.e5

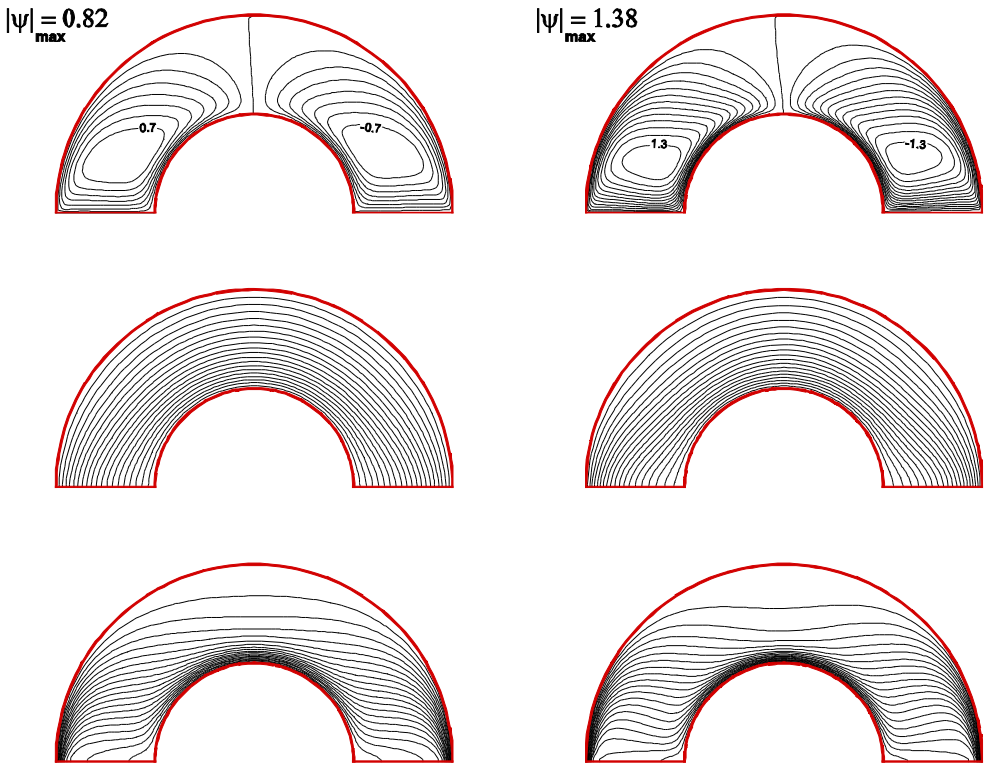

Fig.4 Streamlines (1st row), Isotherms (2nd row) and Iso-concentrations (3rd row) for N=5 (left column) and N=10 (right column) at *Le*=10, *Da*=1.e-4, and *Ra*=1.e5

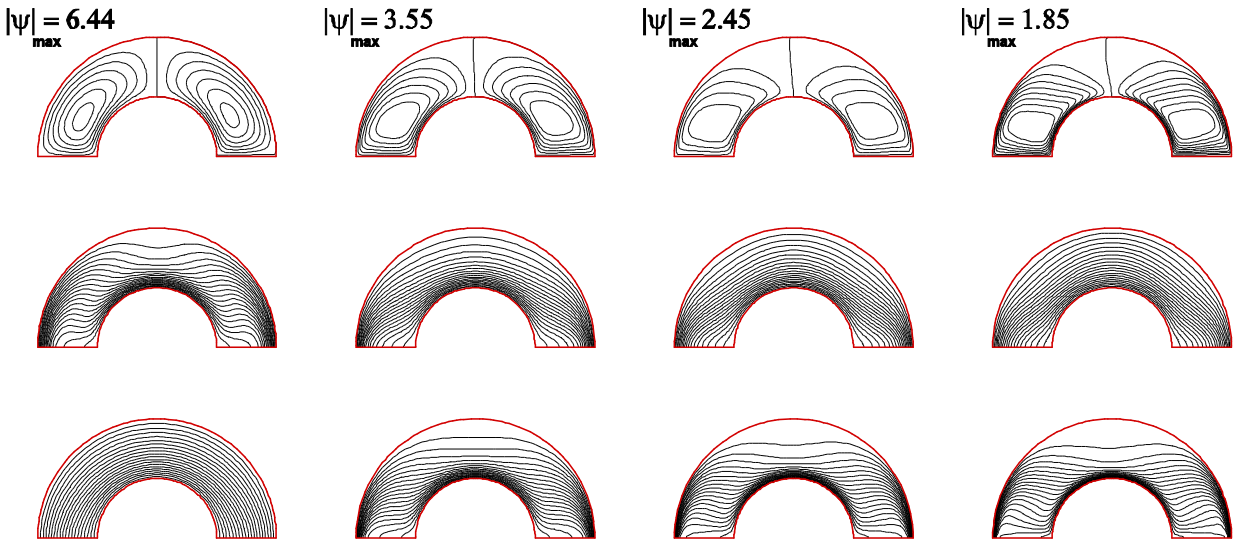

Fig.5 Streamlines (1st row), Isotherms (2nd row) and Iso-concentrations (3rd row) for *Le*=0.1,2,5, and 10 (1st, 2nd, 3rd , 4th columns respectively) at *N*=15, *Da*=1.e-4, and *Ra*=1.e5

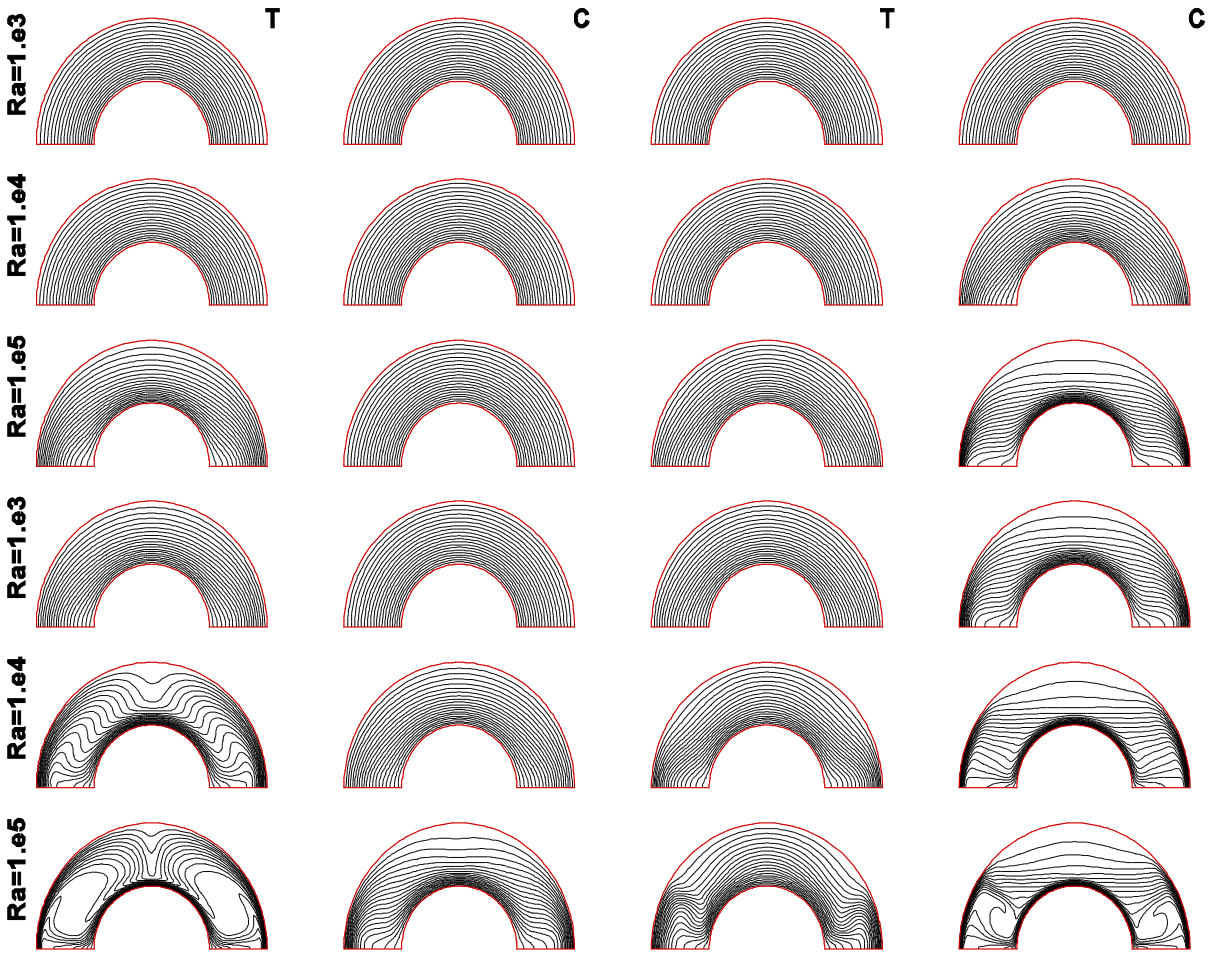

Fig.6 Streamlines and Iso-concentrations at *Da*=1e-4 (3 first rows), *Da*=1e-2 (3 last rows) and *Le*=0.1 (2 first columns), *Le*=10 (2 last columns) for constant *N*=5 and various *Ra* numbers

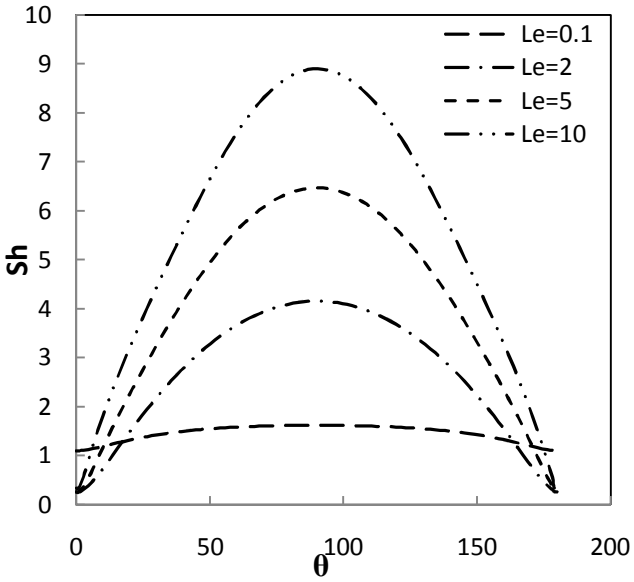

Fig.7 Sherwood number along the hot curved wall for N=10, Ra=1e5, Da=1e-4, and for various Le numbers

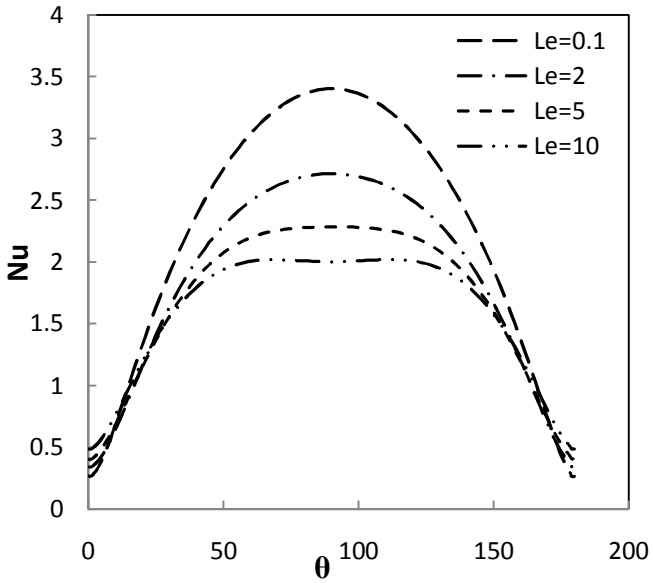

Fig.8 Nusselt number along the hot curved wall for N=10, Ra=1e5, Da=1e-4, and for various Le numbers

Nu decreases with increasing Le. Actually, an increase in the Lewis number decreases the depth of solutal boundary layer leading to amplifying Sherwood number, while it results in a reduction of the flow intensity, which leads to decreasing Nusselt number. Furthermore, it can be seen thet the greater mass transfer rate occurs at the corners of the cavity at Le=0.1, because the mass boundary layer is thinner for this case at the pointed areas.

Figures 9 and 10 exhibit Sherwood number and Nusselt number along the hot curved wall for different values of Le at N=-10. As we know N<0 represents the aiding flow regime. Hence, opposite behavior of the previous graph is expected. In this case, the minimum value occurs in the middle of the cavity, whereas the maximum value occurs in angles 0 and 180 ˚. The minimum value of Sh for Le=0.1 is the greatest one, because the boundary layer is the thinnest for this Le number. For other values of Le, the minimum values are almost equal. Thermal behavior is different, so that from angle 0 to angle 45 Nusselt number augments with an increment in Lewis number, but from angle 45 to angle 90 it reduces with an increment in Lewis number. This behavior recurs for angles between 90 to 180, because the symmetry line locates at the angle of 90.

The effect of buoyancy ratio on average Sherwood number and average Nusselt number for different Lewis numbers are presented in Figures 11 and 12. For aiding flow case (N<0), Nu and Sh decrease with increasing N, but Nu and Sh increase with increasing N at opposing flow case (N>0). The values of Nu and Sh for aiding flows are greater than those of opposing flows at equal absolute value of N, because the magnitude of the velocity and the flow intensity are greater for aiding flows. For instance, at Le=10, for N=-10 (aiding flow)

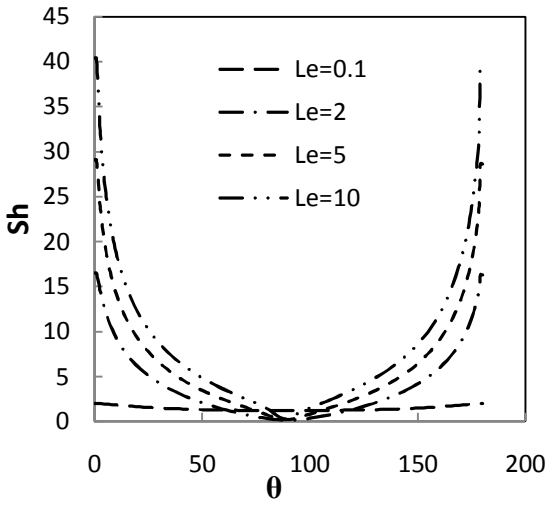

Fig.9 Sherwood number along the hot curved wall for N=-10, Ra=1e5, Da=1e-4, and for various Le numbers

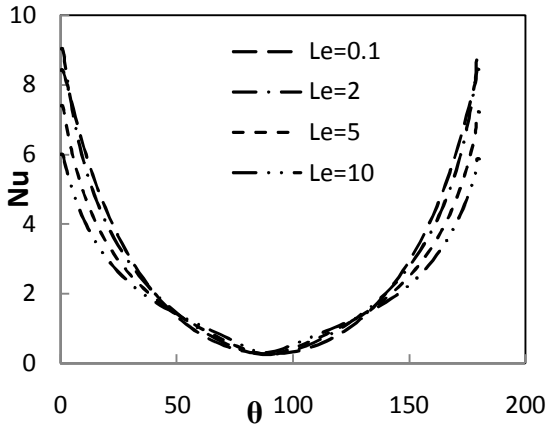

Fig.10 Nusselt number along the hot curved wall for N=-10, Ra=1e5, Da=1e-4, and for various Le numbers

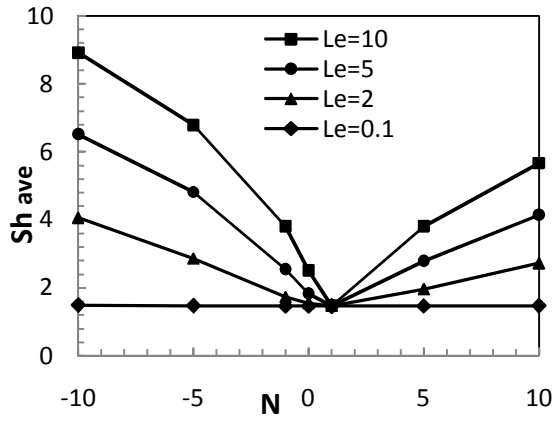

Fig.11 Average Sherwood number along the hot curved wall versus of buoyancy ratio for *Ra*=1e5, *Da*=1e-4, and for various *Le* numbers

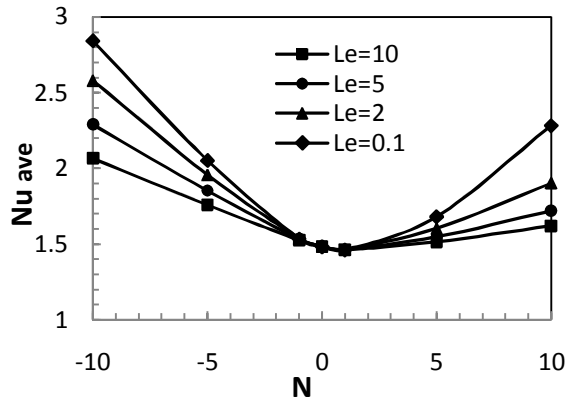

Fig.12 Average Nusselt number along the hot curved wall versus buoyancy ratio for *Ra*=1e5, *Da*=1e-4, and for various *Le* numbers

average Sherwood and Nusselt numbers are 8.93 and 2.84, respectively, while for N=10 (opposing flow) average Sherwood and Nusselt numbers are 5.66 and. 2.28, respectively. Moreover, the figures show that the minimum values in both average Nusselt and Sherwood numbers come about at a buoyancy ratio of 1 (N=1). The last point deduced from the graphs is that for a certain value of N, an increment in the Lewis number, which means an increase of mass diffusivity regarding to thermal diffusivity, results in an increase/decrease of concentration/temperature gradients

5. Conclusions

In the current study, double-diffusive natural convection in a porous arc-shaped enclosure has been numerically studied using Darcy-Brinkman formulation. The impacts of Darcy number, Rayleigh number, Buoyancy ratio, and Lewis number on flow pattern and heat and mass transfer process have been investigated. It was shown for aiding flow ($N<0$) the strength of the flow is greater than that of opposing flow ($N>0$). It leads to greater heat and mass transfers for aiding flow case. Any increment in the Darcy number varies heat and mass profiles visibly, as isotherms and iso-concentrations are distributed in the bulk of the cavity for higher Darcy numbers. An increment in the Lewis number results in an improvement/deterioration of mass/heat transfer process.

Nomenclature

C	*Concentration (Kg m-3)*
C_C	*Concentration at cold wall (Kg m-3)*
C_H	*Concentration at hot wall (Kg m-3)*
D	*Binary diffusion coefficient*
Da	*Darcy number,* K/R^2
Le	*Lewis number,* ν/D
N	*Buoyancy ratio,* $\beta_C \Delta C/\beta_T \Delta T$
Nu	*Local Nusselt number (-)*
Nu_{ave}	*Average Nusselt number (-)*
p	*Dimensionless Pressure (-)*
Pr	*Prandtl number,* ν/α
R	*Radial direction*
Ra	*Rayleigh number,* $g\beta\Delta TR^3/\nu\alpha$
Re	*Reynolds number,* $\rho_f U_0 H/\mu_f$
Sh	*Sherwood number (-)*
T	*Temperature (K)*
T_C	*Temperature of cold wall (K)*
T_H	*Temperature of hot wall (K)*
u	*Velocity (m/s)*

Greek

α	*Thermal diffusivity (m2s-1),* $\kappa/\rho c_p$
β_C	*Coefficient of Thermal expansion (* K^{-1} *)*
β_T	*Coefficient of Solutal expansion (* K^{-1} *)*
ε	*Porosity*
κ	*Thermal conductivity (W/mK)*
μ	*Dynamic viscosity (Nsm-2)*
ν	*Kinematic viscosity (m2s-1),* μ/ρ
θ	*Angular direction*
ρ	*Density (kg/m3)*
ψ	*Stream function*

Superscript

*	*Dimensional parameters*

References

[1]. C.Y. Hu, M.M. EL-Wakil, Simultaneous heat and mass transfer in a rectangular cavity, Proceeding of International Heat Transfer Conference 5 (1974) 24-28.

[2]. S. Ostrach, Natural convection with combined driving forces, Physico Chemical Hydrodynamics 1 (1980) 233-247.

[3]. S.Ostrach, Natural convection heat transfer in cavities and cells, 7th International Heat Transfer Conference 1 (1983) 365-379.

[4]. S. Ostrach, Fluid mechanics in crystal growth-the 1982 freeman scholar lecture, Journal of Fluid Engineering 105 (1983) 5-20.

[5]. T.S. Lee, P.G. Parikh, A. Acrivos, D. Bershader, Natural convection in a vertical channel with opposing buoyancy forces, International Journal of Heat and Mass Transfer 25 (1982) 499-511.
[6]. P. Nithiarasu, T. Sundararajan, K.N. Seetharamu, Double-diffusive natural convection in a fluid saturated porous cavity with a freely convecting wall, International Communications in Heat and Mass Transfer 24 (8) (1997) 1121–1130.
[7]. V.A.F. Costa,Double-diffusive natural convection in parallelogrammic enclosures filled with fluid saturated porous media, International Journal of Heat and Mass Transfer 47 (2004) 2699–2714
[8]. B.Goyeau, J.-P. Songbe and D. Gobin, Numerical study of double-diffusive natural convection in a porous cavity using the Darcy-brinkman formulation, International Journal of Heat and Mass Transfer, 39 (7) (1996), 1363-1378.
[9]. A.J. Chamkha, A. Al-Mudhaf, Double-diffusive natural convection in inclined porous cavities with various aspect ratios and temperature-dependent heat source or sink, Heat and Mass Transfer/Waerme- und Stoffuebertragung 44 (6) (2008) 679–693.
[10]. J.T. Vander Der Eyden, TH. H. Van Der Meer, K. Hanjalic, E. Biezen, J. Bruining, Double-diffusive natural convection in trapezoidal enclosuresm International Journal of Heat and Mass transfer, 41 (13) (1998), 1885-1898.
[11]. M. Bourich, M. Hasnaoui, A. Amahmid, Double-diffusive natural convection in a porous enclosure partially heated from below and differentially salted, International Journal of Heat and Fluid Flow 25 (2004) 1034–1046.
[12]. M.A. Teamah, M.M.Khairat Dawood, M. El-Maghlany, Double-diffusive natural convection in a square cavity with segmental heat sources, European Journal of Scientific Research, 54 (2) (2011), 287-301.
[13]. R. El Ayachi, A. Raji, M. Hasnaoui, A. Abdelbaki, M. Naimi, Resonance of double-diffusive convection in a porous medium heated with a sinusoidal exciting temperature, Journal of Applied fluid Mechanics, 3 (2) (2010), 43-52.
[14]. M. Bourich, A. Amahmid, M. Hasnaoui, Double-diffusive convection in a porous enclosure submitted to cross gradients of temperature and concentration, Energy Conversion and Management, 45 (2004), 1655–1670.
[15]. M.A. Teamah, Double-diffusive laminar natural convection in a symmetrical trapezoidal enclosure, Alexandria Engineering Journal, 45 (3) (2006), 251-263.
[16]. A. Belazizia, S. Benissaad, S. Abboudi, Double-diffusion natural convection of binary fluid in a square enclosure with top Active vertical wall, Advances in Theoretical and Applied Mechanics, 5 (3) (2012), 119-131.
[17]. R. Nikbakhti, A. rahimi, Double-diffusive natural convection in a rectangular cavity with partially thermally active side walls, Journal of the Taiwan Institute of Chemical Engineers 43 (2012) 535–541.
[18]. M.S.Valipour, A.Z. Ghadi, Numerical investigation of fluid flow and heat transfer around a solid circular cylinder utilizing nanofluid, International communications in heat and mass transfer, 38 (2011), 1296-1304.
[19]. S.V. Patankar, Numerical Heat Transfer and Fluid Flow, Hemisphere Publishing Corporation, Washington, 1980.
[20]. H.K. Versteeg, W. Malalasekera, An introduction to computational fluid dynamics. The finite volume method, John Wiley & Sons Inc, New York, 1995.
[21]. R. Iwatsu, J.M. Hyun, K. Kuwahara, Mixed convection in a driven cavity with a stable vertical temperature gradient, International Journal of Heat and Mass Transfer 36 (1993) 1601-1608.